INTERNATIONAL JOURNAL FOR NUMERICAL METHODS IN FLUIDS
Int. J. Numer. Meth. Fluids **26**: 1155–1180 (1998)

METHOD OF FINITE DIFFERENCE SOLUTIONS TO THE TRANSIENT BUBBLY AIR–WATER FLOWS

G. ESPINOSA-PAREDES[a] AND A. SORIA[b,*]

[a] *Instituto de Investigaciones Eléctricas, PO Box 475,Cuernavaca, Mor. 62000, México*
[b] *Departamento de I.P.H., Universidad Autónoma Metropolitana-Iztapalapa, Apdo. 55-534 09340, México*

SUMMARY

A one-dimensional, time-dependent, isothermal, incompressible, Newtonian fluid, two-phase volume averaging model was developed to study momentum interaction effects in vertical ducts with bubble flow regime. For the evaluation of averaged description, potential inviscid flow around bubbles was considered in order to get closure relationships. The linear dynamic analysis is based on the eigenvalue technique, determining the domain of the hyperbolic behavior and the void fraction wave velocity, which are compared with previous models and experimental data. The solution to the partial differential equations is based on the finite difference technique implicit scheme. These schemes serve to demonstrate the numerical solution procedure. The numerical results are compared with analytical solution and experimental data for void fraction wave propagation. The importance of the surface tension effect in the behavior of the phases in transient conditions is shown. © 1998 John Wiley & Sons, Ltd.

KEY WORDS: Navier–Stokes equations; averaged volume transport equations; void wave propagation speed; interfacial effects; two-phase flow; finite difference method

1. INTRODUCTION

One of the main approaches to multiphase flow modelling is the volume averaging of local instantaneous mass, momentum and energy balances, which is developed using spatial and time volume averaging theorems [1–4]. An averaged description should provide enough information for the estimation of the global behavior of the system in terms of averaged variables. The averaging process shows the interaction between the homogeneous regions (phases, interfaces and contact lines) in a multiphase system [5]. The averaged transport equations for multiphase flow can be used to solve several practical problems by analytical means or numerical approaches.

In the present work, a transient local Reynolds time-averaged formulation of gas and liquid phases, with two isothermal, incompressible, Newtonian fluids without phase change, is considered as the starting point for the volume averaging method. The averaging volume selected is a constant, smaller than the size of the whole system and also larger than the size of the bubbles and the separation between adjacent bubbles [6–9]. No wall effects are considered and bubbles are taken as a disperse phase immersed in the liquid. The volume averaged forms of the mass and momentum balance equations for two-phase flow are used for

* Correspondence to: Depto. de I.P.H., Universidad Autónoma Metropolitana-Iztapalapa, Apdo. 55-534, 09340 México, O.F., México.

CCC 0271–2091/98/101155–26$17.50

Received August 1996
Revised May 1997

the analysis of momentum interaction effects between phases under steady state and transient conditions.

A methodical closure procedure was performed in order to get a closed set of continuity and momentum averaged equations. The closure was formulated as an associated problem for the deviations around averaged values of the local variables. A particular system of spherical non-interacting bubbles and potential inviscid flow around bubbles was considered, in order to get closure relationships [10]. The interfacial effects include drag, virtual mass, covariant Reynolds stress induced by bubbles, interfacial averaged pressure and surface tension.

When the dispersion of gas bubbles in a continuous liquid phase is represented by two separated fluids, each having its own motion equation, instabilities may arise in the computational step. Computational instabilities are related to the complex characteristic roots [11–13]. This means that the theoretical initial-value problem is in general ill-posed, because small perturbations of the initial value may grow without limit during the evaluation in time of the two-phase flow system [11]. On the other hand, complex characteristic roots may be attributed to physical instabilities in flow transitions, such as those from bubble flow to churn or slug flow, driven by bubble interactions and coalescence [14,15]. It should be stressed that, according to the requirements of the volume averaging method considered, the occurrence of such instabilities should set the limits of application of the model. This is due to the fact that the imposed length scale restrictions are no longer satisfied following the transition to churn or slug flow regimes, where the number of bubbles is greatly decreased and their size is increased to lengths in the order of magnitude of the characteristic length of the whole system, e.g. the pipe diameter [14]. A linear analysis and propagation of void waves are performed in the present work, with the evaluation of characteristics roots, which represent the fastest and slowest kinematic wave velocities in the system [16].

The solution for the two-fluid model in order to obtain the velocities, pressures and void fraction distributions as functions of time and position, is based on a finite difference technique implicit scheme. This scheme serves to demonstrate the numerical solution procedure. The system is a column, 1 m in vertical length. A one-dimensional, 100 cell, mesh-centered grid, consisting of a variable number of axial elements, is used. The concept of donor cell is used for parameter lumping purposes. Stability of the numerical solutions is improved using this concept. The integration step used for this model was 1/100 of a second. The results were compared with experimental data on void propagation in bubbly flows [17,18] and with an analytic solution taking different sets of superficial velocity conditions.

The interfacial terms are an essential feature of momentum balances. If interfacial terms are restricted to the interfacial pressure difference for the liquid phase and the interfacial drag force, a basic numerical solution can be obtained. Other interfacial and bulk mechanisms can also be considered. In addition, Reynolds stresses slightly modify the basic solution. Conversely, added mass terms contribute highly to the reduction of the slip between phases, because added mass terms involve both the deceleration of gas phase by the liquid and the continuation of liquid by gas bubbles. Lahey *et al.* [19] found that the final numerical results were insensitive to the virtual mass effect, but the numerical stability and efficiency were greatly improved. This effect changes the value of the eigenvalues of the two-fluid model, enlarging the real eigenvalue zone.

Surface tension effects are known to substantially influence the behavior of multiphase dispersed systems and were considered to be the source and flux terms located at the interface [5,20]. In the present work, the surface tension effect was explicitly considered. This effect was found to be significant, because its absence causes the deceleration of the gas phase and is very important in the determination of the hyperbolicity domain. This effect has not been considered in previous analyses on void propagation in bubbly flows.

2. MICROSCOPIC TO MACROSCOPIC VARIABLES THROUGH VOLUME AVERAGING

Bubbling flow through a vertical duct is represented in Figure 1. While Reynolds time averaged Navier–Stokes equations can be applied to liquid and gas Newtonian fluid phases, both phases are moving and the application domain of such an equation is unknown. Therefore, considering both phases as an effective mixture of fluids may be preferred, but additional assumptions and developments must be made in order to describe such two-phase mixtures. One of the available techniques to obtain the two-phase flow model is the volume averaging method. This method can be considered as a mathematical technique which allows the transformation from local field variables to averaged field variables, using a volume averaging operator. Averaging equations are not dependent on local variables such as the size and/or velocity of the individual bubbles, but only on the averaged field variables, once an appropriate closure scheme has been performed. The averaging method has been applied to both laminar flows [25,31] and turbulent flows [26,32]. The application of the averaging method to turbulent flows needs a previous step of time averaging in order to use the Reynolds averaged Navier–Stokes equations. This leads to the establishment and the closure of turbulent flow before application of the volume averaging technique.

The system is composed of a continuous liquid phase (water) and a disperse gas phase (air) made up of a swarm of spherical bubbles. The system is taken to be isothermal and the vertical duct has a diameter much greater than the size of the individual bubbles. Both phases are considered locally incompressible and without interfacial mass transfer. Interfacial momentum transfer is allowed and a constant surface tension is given. The mixture of gas and liquid is assumed to be either far away from the solid walls of the duct or to present small viscous effects near the wall, in such a way that wall effects can be neglected.

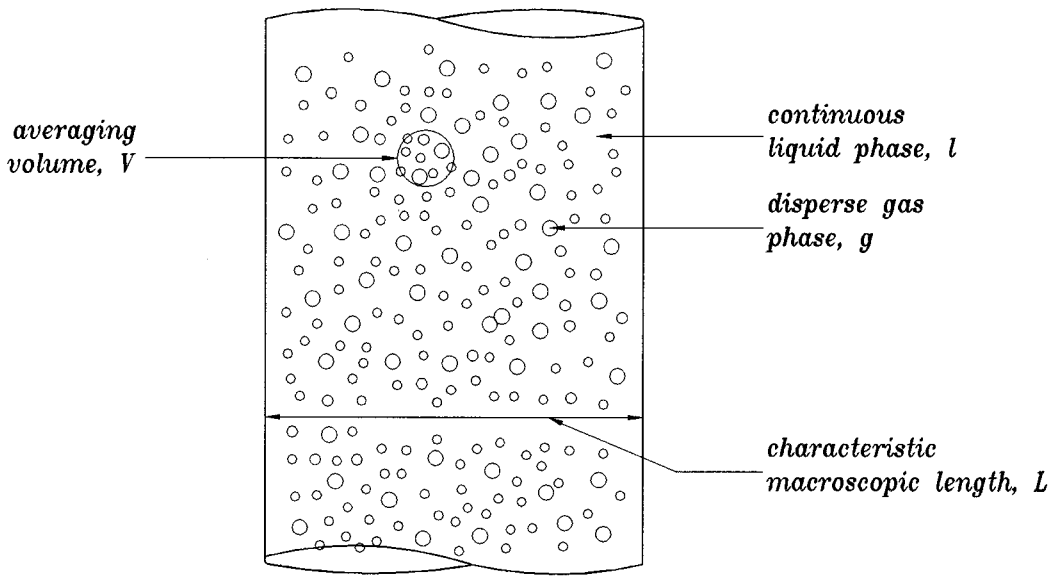

Figure 1. Macroscopic system and hypothetical averaging volume with two phases present.

2.1. Local equations

Local equations for mass and momentum transfers, as well as interfacial jump conditions, are given by the following set:

Continuity equation for phase k

$$\nabla \cdot \bar{\boldsymbol{v}}_k = 0, \tag{1}$$

where k is the liquid (l) and gas (g) phases.

Momentum equation for phase k

$$\rho_k \frac{\partial \bar{\boldsymbol{v}}_k}{\partial t} + \rho_k \nabla \cdot (\bar{\boldsymbol{v}}_k \bar{\boldsymbol{v}}_k) + \nabla \cdot (\bar{p}_k \boldsymbol{I}) - \nabla \cdot \bar{\boldsymbol{\tau}}_k^T - \rho_k \boldsymbol{g}_k = 0, \tag{2}$$

where ρ_k, $\boldsymbol{v}_k$, p_k, $\boldsymbol{\tau}_k^T$ are the local variables in the k-phase, representing density, velocity vector, pressure and total (laminar and turbulent) stress tensor respectively; $\boldsymbol{I}$ represents a unit tensor and $\boldsymbol{g}_k$ is the acceleration of gravity vector.

Interfacial impenetrability condition

$$\overline{(\boldsymbol{v}_k - \boldsymbol{v}_\mathrm{i}) \cdot \boldsymbol{n}_{k\mathrm{i}}} = 0, \quad \text{at } A_\mathrm{i}, \tag{3}$$

where $\boldsymbol{v}_\mathrm{i}$ is the velocity vector of the interface, $\boldsymbol{n}_{k\mathrm{i}}$ is the unit vector normal to the interface pointing out of phase k and A_i represents the interface surface contained in the macroscopic region (Figure 2).

Interfacial momentum jump condition

$$\sum_{k=\mathrm{l,g}} \overline{(-p_k \boldsymbol{n}_{k\mathrm{i}} + \boldsymbol{\tau}_k \cdot \boldsymbol{n}_{k\mathrm{i}})} = 2\overline{H_\mathrm{g} \boldsymbol{n}_{\mathrm{gi}}}\sigma, \quad \text{at } A_\mathrm{i}, \tag{4}$$

where σ is the interfacial tension and H_g is the mean curvature of the interface ($2H_\mathrm{g} = -\nabla \cdot \boldsymbol{n}_{\mathrm{gi}}$).

Particular solutions also require the values of inlet and initial conditions:

$$\text{BC1} \quad \bar{\boldsymbol{v}}_k = f(\boldsymbol{x}, t), \quad \text{at } A_{k\mathrm{e}}, \tag{5}$$

$$\text{BC2} \quad \bar{p}_k = \bar{p}_k(\boldsymbol{x}), \quad \text{at } \boldsymbol{x} = \boldsymbol{x}_0, \tag{6}$$

$$\text{IC1} \quad \bar{\boldsymbol{v}}_k = g(\boldsymbol{x}), \quad \text{at } t = 0, \tag{7}$$

where $\boldsymbol{x}$ is the position vector and $A_{k\mathrm{e}}$ represents the k-phase entrances and exits associated with the macroscopic region.

2.2. Volume averaged variables

The previous local set of equations cannot be solved for a system with an unknown number of bubbles moving in the liquid. In order to obtain such an averaged description, an integral volume averaging operator should be applied to the local equations. The averaging volume selected is a constant, smaller than the size of the whole system and also larger than the size of the bubbles and the separation between adjacent bubbles, as can be observed in Figure 2, where l_g and l_l are the characteristic lengths of gas and liquid phases respectively, r_0 is the characteristic length of the averaging volume and L is the characteristic macroscopic length of the duct [6–8].

In order to obtain meaningful averaged quantities, the characteristic length of the averaging volume, must satisfy the inequality [6]

$$l_k \ll r_0 \ll L. \tag{8}$$

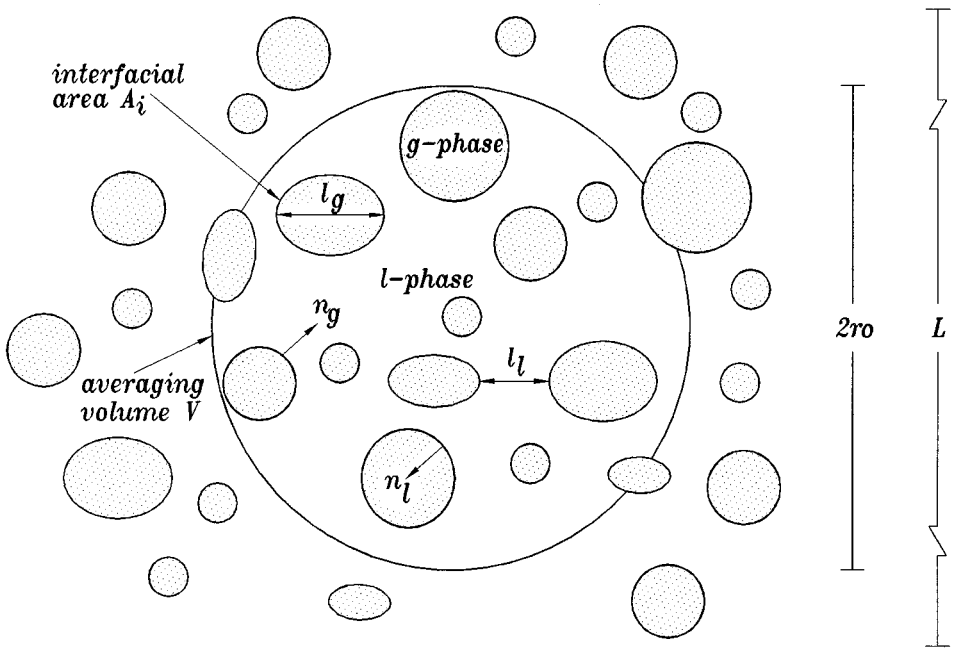

Figure 2. Macroscopic region (L), and averaging volume (V). Here r_0 is the radius of the averaging volume, l_g and l_l are small lengths, $\boldsymbol{n}_g$ and $\boldsymbol{n}_l$ are the unit normal vectors.

If the foregoing inequality does not hold, or if the scale of the problem of interest is of order r_0, the averaging technique and therefore, the macroscopic theories of multiphase flow should be modified in order to include appropriate considerations and terms in the corresponding equations.

2.3. Averaging operators

Up to this point, Reynolds turbulent variables have been denoted by a bar above the corresponding symbol. In order to simplify the notation the bar is omitted from this point on.

For the averaging procedure described in this study, the averaging operator for a general variable ψ_k is defined as

$$\langle \psi_k \rangle = \frac{1}{V} \int_{R_k(t)} \psi_k \, \mathrm{d}V, \tag{9}$$

which is known as a *phase average*. The *intrinsic phase average* is given by

$$\langle \psi_k \rangle^k = \frac{1}{V_k} \int_{R_k(t)} \psi_k \, \mathrm{d}V, \tag{10}$$

where, $R_k(t) \subset \mathbb{R}^3$ is the region occupied by phase k and $V_k(t)$ represents the volume of the k-phase associated with region $R_k(t)$. The phase average and intrinsic phase average are related by

$$\langle \psi_k \rangle = \varepsilon_k \langle \psi_k \rangle^k, \tag{11}$$

where $\varepsilon_k(t)$ is the volume fraction, explicitly defined by $V_k(t)/V$. In order to present the volume average of Equations (1) and (2), two special averaging theorems are needed. The first one is the time averaging theorem given by [1,2]

$$\left\langle \frac{\partial \psi_k}{\partial t} \right\rangle = \frac{\partial \langle \psi_k \rangle}{\partial t} - \frac{1}{V} \int_{A_i(t)} \psi_k \boldsymbol{v}_i \cdot \boldsymbol{n}_{ki} \, dA. \tag{12}$$

The second integral theorem is known as the spatial averaging theorem. For some scalar quantity ψ_k associated with the k-phase, this theorem is given by [1,2,4]

$$\langle \nabla \psi_k \rangle = \nabla \langle \psi_k \rangle + \frac{1}{V} \int_{A_i(t)} \psi_k \boldsymbol{n}_{ki} \, dA. \tag{13}$$

If ψ_k is 1, the previous theorems give

$$\frac{\partial \varepsilon_k}{\partial t} = \frac{1}{V} \int_{A_i(t)} \boldsymbol{n}_{ki} \cdot \boldsymbol{v}_i \, dA, \tag{14}$$

$$\nabla \varepsilon_k = -\frac{1}{V} \int_{A_i(t)} \boldsymbol{n}_{ki} \, dA. \tag{15}$$

2.4. Averaged mass equation

The local mass equation given by Equation (1), may be volume averaged using the operators given above. The result is

$$\frac{\partial \varepsilon_k}{\partial t} + \varepsilon_k \nabla \cdot \langle \boldsymbol{v}_k \rangle^k + \langle \boldsymbol{v}_k \rangle^k \cdot \nabla \varepsilon_k = 0. \tag{16}$$

The terms of this equation are related to macroscopic compressibility and convective effects.

2.5. Averaged momentum equation

The transient Reynolds momentum equation (2) is volume averaged as follows. First, the time and spatial averaging theorems given by Equations (12) and (13) respectively, are applied. Then, variations in ρ_k within the averaging volume are ignored because density is a parameter that does not often change in large volumes of flow. Moreover, an order of magnitude analysis shows that the interfacial stresses are much greater than the bulk stresses. This can be observed by a numerical comparison shown in Table I, from data reported by Wang *et al.* [49]

In Table I, the values of bulk stresses in the pipe core were compared with the interfacial stresses for several void fraction values. Comparison of both kinds of stresses is possible since the same operation range has been used for both sets of values. It is apparent that interfacial stresses are far more important than bulk stresses. The same conclusion can be drawn up by an order of magnitude analysis as follows:

Table I. Comparison of interfacial stresses and bulk stresses

ε_g	$1/V \int_{A_i(t)} \boldsymbol{n}_{ki} \cdot \boldsymbol{\tau}_{ki}^T \, dA$	$\langle v_g \rangle$ (m s^{-1})	$\nabla \cdot \langle \boldsymbol{\tau}_k^T \rangle$ [49]
0.4	9324	0.4	2.6
0.3	8632	0.27	1.53
0.2	8075	0.10	1.18
0.1	7613	0	0.82

$$\nabla \cdot \langle \boldsymbol{\tau}_k^T \rangle = \boldsymbol{O}\left(\frac{\langle \boldsymbol{\tau}_k^T \rangle}{L_\tau} \right), \tag{17}$$

$$\frac{1}{V} \int_{A_i(t)} \boldsymbol{n}_{ki} \cdot \boldsymbol{\tau}_{ki}^T \, \mathrm{d}A = \boldsymbol{O}\left[\frac{(l_g/\delta)\langle \boldsymbol{\tau}_k^T \rangle}{L_\varepsilon} \right]. \tag{18}$$

In Equations (17) and (18), δ is the liquid boundary layer thickness on the surface of the bubble where the viscous stresses act, and L_τ and L_ε are characteristic lengths associated with changes in $\langle \tau_k^T \rangle$ and changes in ε_k, respectively. Since (l_g/δ) is much larger than one and $L_\tau = \boldsymbol{O}(L_\varepsilon)$, the term $\nabla \cdot \langle \tau_k^T \rangle$ in Equation (17) is much smaller than the interfacial stresses, given by the left-hand side of (18).

With these considerations, the following form of the averaged momentum equation is obtained:

$$\rho_k \frac{\partial}{\partial t} (\varepsilon_k \langle \boldsymbol{v}_k \rangle^k) + \rho_k \nabla \cdot (\varepsilon_k \langle \boldsymbol{v}_k \boldsymbol{v}_k \rangle^k) + \nabla (\varepsilon_k \langle p_k \rangle^k) - \varepsilon_k \rho_k \boldsymbol{g}_k$$
$$= -\frac{1}{V} \int_{A_i(t)} p_k \boldsymbol{n}_{ki} \, \mathrm{d}A + \frac{1}{V} \int_{A_i(t)} \boldsymbol{n}_{ki} \cdot \boldsymbol{\tau}_{ki}^T \, \mathrm{d}A, \tag{19}$$

where the relationship between phase averaging and intrinsic phase averaging given by Equation (11) has been considered, as well as the condition for interfacial null mass transfer, (3). The terms of Equation (19) involve integrals as well as products of the local variables. The second term on the left-hand side of Equation (19) requires the use of spatial decomposition [21,22].

$$\boldsymbol{v}_k = \langle \boldsymbol{v}_k \rangle^k + \tilde{\boldsymbol{v}}_k. \tag{20}$$

Substitution of Equation (20) in the convective term of (19) gives rise to an averaged convective term together with a convective covariance term, known as the Reynolds stress (τ_k^{Re}) in the field literature [10,23,24]

$$\rho_k \nabla \cdot (\varepsilon_k \langle \boldsymbol{v}_k \boldsymbol{v}_k \rangle^k) = \rho_k \nabla \cdot (\varepsilon_k \langle \boldsymbol{v}_k \rangle^k \langle \boldsymbol{v}_k \rangle^k) - \nabla \cdot (\varepsilon_k \tau_k^{Re}). \tag{21}$$

On the other hand, Banerjee [25] decomposes the local pressure as the following sum:

$$p_k = \langle p_k \rangle^k + \langle \Delta p_{ki} \rangle + \tilde{p}_{ki}, \tag{22}$$

where the difference between the intrinsic interfacial average pressure and the intrinsic average pressure for the k-phase is

$$\langle \Delta p_{ki} \rangle = \frac{1}{A_i} \int_{A_i(t)} p_k \, \mathrm{d}A - \frac{1}{V_k} \int_{R_k(t)} p_k \, \mathrm{d}V = \langle p_k \rangle_i - \langle p_k \rangle^k, \tag{23}$$

and the deviation from the interfacial average is

$$\tilde{p}_{ki} = p_k - \langle p_k \rangle_i. \tag{24}$$

This decomposition has the advantage of distinguishing the contributions of the momentum exchange terms. Substituting Equations (21) and (22) into (19), the final form of the volume averaged momentum equations is obtained:

$$\rho_k \frac{\partial}{\partial t} (\varepsilon_k \langle \boldsymbol{v}_k \rangle^k) + \rho_k \nabla \cdot (\varepsilon_k \langle \boldsymbol{v}_k \rangle^k \langle \boldsymbol{v}_k \rangle^k) + \varepsilon_k \nabla \langle p_k \rangle^k - \langle \Delta p_{ki} \rangle \nabla \varepsilon_k - \nabla \cdot (\varepsilon_k \boldsymbol{\tau}_k^{Re}) - \varepsilon_k \rho_k \boldsymbol{g}_k$$
$$= -\frac{1}{V} \int_{A_i(t)} \tilde{p}_{ki} \boldsymbol{n}_{ki} \, \mathrm{d}A + \frac{1}{V} \int_{A_i(t)} \boldsymbol{n}_{ki} \cdot \boldsymbol{\tau}_{ki}^T \, \mathrm{d}A. \tag{25}$$

2.6. Interfacial jump condition

The local jump conditions (Equations (3) and (4)), can be volume averaged as previously done with the phase transport equations. The interfacial mass jump condition is null according to the impenetrability condition given by Equation (3), and the interface momentum jump condition (4) takes the form (after averaging):

$$(\langle p_l\rangle_i - \langle p_g\rangle_i)\nabla\varepsilon_g = \sum_{k=l,g}\left(\frac{1}{V}\int_{A_i(t)}(-\tilde{p}_{ki}\boldsymbol{n}_{ki} + \boldsymbol{n}_{ki}\cdot\boldsymbol{\tau}_{ki}^T)\,dA\right) + 2\langle H_g\rangle_i\sigma\nabla\varepsilon_g + \frac{1}{V}\int_{A_i(t)} 2\tilde{H}_g\sigma\boldsymbol{n}_{gi}\,dA. \tag{26}$$

The first integral contains both non-drag effects (virtual mass forces and lateral lift forces) and drag effects (interfacial drag forces) [26]. This integral can be expressed by the symbol $\boldsymbol{M}_{ki}$, defined as the interfacial force per unit volume of phase k. The previous equation can be rewritten as

$$(\langle p_l\rangle_i\langle p_g\rangle_i)\nabla\varepsilon_g = \boldsymbol{M}_{li} + \boldsymbol{M}_{gi} + 2\sigma\langle H_g\rangle_i\nabla\varepsilon_g + \frac{1}{V}\int_{A_i(t)} 2\sigma\tilde{H}_g\boldsymbol{n}_{gi}\,dA. \tag{27}$$

3. ONE-DIMENSIONAL AVERAGED TRANSPORT EQUATIONS

The one-dimensional averaged transport equations can be derived from the three-dimensional volume averaged transport equations for two-phase flow, given previously. This can be accomplished for the vectorial momentum equations by a dot product with a unit vector $\boldsymbol{e}_z$ in the axial co-ordinate direction of a polar cylindrical co-ordinate system. The following set of volume averaged equations is then obtained for a one-dimensional two-phase bubbling flow. One-dimensional averaged mass transport equation (16) becomes

$$\frac{\partial\varepsilon_k}{\partial t} + \varepsilon_k\frac{\partial}{\partial z}\langle v_{zk}\rangle^k + \langle v_{zk}\rangle^k\frac{\partial\varepsilon_k}{\partial z} = 0; \quad k = l, g, \tag{28}$$

where it has been assumed that

$$\langle \boldsymbol{v}_k\rangle^k = \boldsymbol{e}_z\langle v_{zk}\rangle^k(z). \tag{29}$$

One-dimensional averaged momentum equation (25), projected onto the $\boldsymbol{e}_z$-direction, gives

$$\rho_k\frac{\partial}{\partial t}(\varepsilon_k\langle v_{zk}\rangle^k) + \rho_k\frac{\partial}{\partial z}(\varepsilon_k\langle v_{zk}\rangle^k\langle v_{zk}\rangle^k) + \varepsilon_k\frac{\partial}{\partial z}\langle p_k\rangle^k - \langle\Delta p_{ki}\rangle\frac{\partial}{\partial z}\varepsilon_k + \varepsilon_k\rho_k g = \frac{\partial}{\partial z}(\varepsilon_k\tau_{zzk}^{Re}) + M_{ki}; \quad k = l, g, \tag{30}$$

where, according to Equation (25), the interfacial force on phase k is given by

$$M_{ki} = -\frac{1}{V}\int_{A_i(t)}\boldsymbol{e}_z\cdot\boldsymbol{n}_{ki}\tilde{p}_{ki}\,dA + \frac{1}{V}\int_{A_i(t)}\boldsymbol{e}_z\cdot\boldsymbol{n}_{ki}\cdot\boldsymbol{\tau}_{ki}^T\,dA, \tag{31}$$

and it has also been considered that

$$\boldsymbol{\tau}_k^{Re} = \boldsymbol{e}_z\boldsymbol{e}_z\tau_{zzk}^{Re}. \tag{32}$$

In order to solve this set of equations, it is imperative to propose appropriate closure relationships for the terms (Δp_{ki}), τ_{zzk}^{Re}, M_{ki}. This is the purpose of the following section.

4. CLOSURE RELATIONSHIPS AND COMPLETE SET OF EQUATIONS

As a first approximation for the evaluation of the previous averaged description, potential flow around bubbles was considered in order to get closure relationships. Further contributions will develop closures for low Reynolds number flows, where the importance of averaged viscous terms should be enhanced.

The momentum transfer between the gas and liquid phases for each phase is given by Equation (31). For a dilute bubble flow this equation can be represented as a summation of several forces on an object immersed in a fluid [26]. The main contributions are the two forces considered here:

$$M_{\mathrm{li}} = \varepsilon_{\mathrm{g}}(F_{\mathrm{D}} + F_{\mathrm{VM}}), \tag{33}$$

where the interfacial drag force accounts for the interfacial shear stresses. For a bubbly flow with uniform bubble size, the axial component of this force, F_{D} is given by [27].

$$F_{\mathrm{D}} = \frac{1}{V}\int_{A_{\mathrm{i}}(t)} \boldsymbol{e}_z \cdot \boldsymbol{n}_{k\mathrm{i}} \cdot \boldsymbol{\tau}_{k\mathrm{i}}\, \mathrm{d}A = \frac{3}{8}\rho_{\mathrm{l}}\frac{C_{\mathrm{D}}}{R_{\mathrm{b}}}(\langle v_{z\mathrm{g}}\rangle^{\mathrm{g}} - \langle v_{z\mathrm{l}}\rangle^{\mathrm{l}})\left|\langle v_{z\mathrm{g}}\rangle^{\mathrm{g}} - \langle v_{z\mathrm{l}}\rangle^{\mathrm{l}}\right|, \tag{34}$$

where R_{b} is the equivalent bubble radius, and the drag coefficient, C_{D} for distorted bubbly flows, is given by [28]

$$C_{\mathrm{D}} = \frac{4}{3}R_{\mathrm{b}}\left[\frac{g(\rho_{\mathrm{l}} - \rho_{\mathrm{g}})}{\sigma(1-\varepsilon_{\mathrm{g}})}\right]^{1/2}. \tag{35}$$

This drag coefficient was found to fit our tests appropriately, compared with the drag coefficient for undistorted bubbles. A similar behavior was found by Ruggles *et al.* [29]. A detailed analysis on the two-phase drag coefficient is reported by Ishii and Mishima [27].

The virtual mass force, F_{VM} is given by

$$F_{\mathrm{VM}} = -\frac{1}{V}\int_{A_{\mathrm{i}}(t)} \boldsymbol{e}_z \cdot \boldsymbol{n}_{k\mathrm{i}}\tilde{p}_{k\mathrm{i}}\, \mathrm{d}A = \rho_{\mathrm{l}} C_{\mathrm{VM}} a_{\mathrm{VM}}, \tag{36}$$

where the magnitude of the virtual mass acceleration, a_{VM}, for one-dimensional models is given by [23,30,31]

$$a_{\mathrm{VM}} = \left(\frac{\partial\langle v_{z\mathrm{g}}\rangle^{\mathrm{g}}}{\partial t} + \langle v_{z\mathrm{g}}\rangle^{\mathrm{g}}\frac{\partial\langle v_{z\mathrm{g}}\rangle^{\mathrm{g}}}{\partial z}\right) - \left(\frac{\partial\langle v_{z\mathrm{l}}\rangle^{\mathrm{l}}}{\partial t} + \langle v_{z\mathrm{l}}\rangle^{\mathrm{l}}\frac{\partial\langle v_{z\mathrm{l}}\rangle^{\mathrm{l}}}{\partial z}\right). \tag{37}$$

The virtual volume coefficient for single spherical particles is $C_{\mathrm{VM}} = 1/2$. For different shapes, C_{VM} is a shape-dependent parameter.

The interfacial pressure, given by Drew [10], is based on the potential flow theory for inviscid flow and Bernoulli's equations for an incompressible fluid around a sphere of constant radius:

$$\langle \Delta p_{\mathrm{li}}\rangle = \langle p_{\mathrm{l}}\rangle_{\mathrm{i}} - \langle p_{\mathrm{l}}\rangle^{\mathrm{l}} = -\xi\rho_{\mathrm{l}}(\langle v_{z\mathrm{g}}\rangle^{\mathrm{g}} - \langle v_{z\mathrm{l}}\rangle^{\mathrm{l}})^2, \tag{38}$$

where $\xi = 1/4$ for dilute flows. A particular model, considering surface tension effects, can be proposed by taking

$$\langle p_{\mathrm{g}}\rangle^{\mathrm{g}} - \langle p_{\mathrm{l}}\rangle^{\mathrm{l}} = \sigma\langle H_{\mathrm{g}}\rangle_{\mathrm{i}} - \xi\rho_{\mathrm{l}}(\langle v_{z\mathrm{g}}\rangle^{\mathrm{g}} - \langle v_{z\mathrm{l}}\rangle^{\mathrm{l}})^2, \tag{39}$$

where $\langle H_{\mathrm{g}}\rangle_{\mathrm{i}}$ is the mean curvature of the interface, which is given by [33]

$$\langle H_g \rangle_i = \frac{2}{R_b}. \tag{40}$$

The average pressure at the interface and the intrinsic average pressure for the gas phase are taken to be equal, i.e.

$$\langle p_g \rangle_i \cong \langle p_g \rangle^g. \tag{41}$$

This assumption is valid, as the average pressure within a bubble is very close to its interfacial average pressure. Another assumption is that the interfacial average pressure for both phases is uniform, with a constant surface tension [24,32]. This assumption implies some simplifications on the momentum jump condition, rewritten from Equation (27) as follows:

$$M_{gi} = (\langle p_l \rangle_i - \langle p_g \rangle^g) \frac{\partial \varepsilon_g}{\partial z} - M_{li} + 2\sigma \langle H_g \rangle_i \frac{\partial \varepsilon_g}{\partial z} - \frac{1}{V} \int_{A_i(t)} 2\sigma \tilde{H}_g \boldsymbol{e}_z \cdot \boldsymbol{n}_{gi} \, dA. \tag{42}$$

The main assumptions to be considered here are: (1) The last term in Equation (42) can be taken as negligible if the distribution of bubbles is close to a single-sized distribution and, (2) quasi-static conditions, given by Equation (39) can be assumed. Then

$$M_{gi} = -\sigma \frac{2}{R_b} \frac{\partial \varepsilon_g}{\partial z} - M_{li}. \tag{43}$$

Bubbles induce turbulence on the liquid phase. This fact is accounted for by liquid Reynolds stresses, given by [10]

$$\tau_{zzl}^{Re} = -k\rho_l \varepsilon_g (\langle v_{zg} \rangle^g - \langle v_{zl} \rangle^l)^2, \tag{44}$$

where $k = 1/5$. The Reynolds stresses in the gas phase can be taken equal to zero, i.e.

$$\tau_{zzg}^{Re} \cong 0, \tag{45}$$

because the turbulence inside bubbles can be neglected.

4.1. Complete set of equations

The present set of four independent equations, (28) and (30) for $k = 1$, g, has two degrees of freedom, because there are six unknowns: ε_g, ε_l, $\langle v_{zg} \rangle^g$, $\langle v_{zl} \rangle^l$, $\langle p_g \rangle^g$ and $\langle p_l \rangle^l$. The so-called 'saturation condition':

$$\varepsilon_g + \varepsilon_l = 1 \tag{46}$$

is a complementary relationship. One more expression can be obtained by derivation of the closure Equation (39) with respect to z, then

$$\frac{\partial}{\partial z} \langle p_g \rangle^g = \frac{\partial}{\partial z} \langle p_l \rangle^l - 2\xi \rho_l (\langle v_{zg} \rangle^g - \langle v_{zl} \rangle^l) \left(\frac{\partial}{\partial z} \langle v_{zg} \rangle^g - \frac{\partial}{\partial z} \langle v_{zl} \rangle^l \right). \tag{47}$$

Substituting Equation (46) into (28) and (30) for $k = l$, substituting Equation (48) into (30) for $k = g$, and substituting closure relationships given in the previous section, reduces the system to a closed set of four equations with four unknowns: ε_g, $\langle v_{zg} \rangle^g$, $\langle v_{zl} \rangle^l$ and $\langle p_l \rangle^l$. These equations are

$$\frac{\partial \varepsilon_g}{\partial t} + \varepsilon_g \frac{\partial}{\partial z} \langle v_{zg} \rangle^g + \langle v_{zg} \rangle^g \frac{\partial \varepsilon_g}{\partial z} = 0 \quad \text{in the g-phase,} \tag{48}$$

$$\frac{\partial \varepsilon_g}{\partial t} - \varepsilon_l \frac{\partial}{\partial z}\langle v_{zl}\rangle^l + \langle v_{zl}\rangle^l \frac{\partial \varepsilon_g}{\partial z} = 0 \quad \text{in the l-phase,} \tag{49}$$

$$\rho_g \langle v_{zg}\rangle^g \frac{\partial \varepsilon_g}{\partial t} + (\varepsilon_g \rho_g + K_{VM}) \frac{\partial}{\partial t}\langle v_{zg}\rangle^g - K_{VM} \frac{\partial}{\partial t}\langle v_{zl}\rangle^l + [\rho_g(\langle v_{zg}\rangle^g)^2 + \sigma \langle H_g\rangle_i] \frac{\partial \varepsilon_g}{\partial z}$$
$$+ [2\varepsilon_g(\rho_g \langle v_{zg}\rangle^g - \xi \rho_l v_r) + K_{VM}\langle v_{zg}\rangle^g] \frac{\partial}{\partial z}\langle v_{zg}\rangle^g + (2\xi \varepsilon_g \rho_l v_r - K_{VM}\langle v_{zl}\rangle^l) \frac{\partial}{\partial z}\langle v_{zl}\rangle^l$$
$$+ \varepsilon_g \frac{\partial}{\partial z}\langle p_l\rangle^l = -\varepsilon_g \rho_g g - \varepsilon_g F_D \quad \text{in the g-phase,} \tag{50}$$

$$-\rho_l \langle v_{zl}\rangle^l \frac{\partial \varepsilon_g}{\partial t} - K_{VM} \frac{\partial}{\partial t}\langle v_{zg}\rangle^g + (\rho_l \varepsilon_l + K_{VM}) \frac{\partial}{\partial t}\langle v_{zl}\rangle^l - \rho_l[(\langle v_{zl}\rangle^l)^2 + v_r^2(\xi + k(\varepsilon_g - \varepsilon_l))] \frac{\partial \varepsilon_g}{\partial z}$$
$$+ (2k\rho_l \varepsilon_l \varepsilon_g v_r - K_{VM}\langle v_{zg}\rangle^g) \frac{\partial}{\partial z}\langle v_{zg}\rangle^g + [2\varepsilon_l \rho_l(\langle v_{zl}\rangle^l - k\varepsilon_g v_r) + K_{VM}\langle v_{zl}\rangle^l] \frac{\partial}{\partial z}\langle v_{zl}\rangle^l$$
$$+ \varepsilon_l \frac{\partial}{\partial z}\langle p_l\rangle^l = -\varepsilon_l \rho_l g + \varepsilon_g F_D \quad \text{in the l-phase,} \tag{51}$$

where the following equalities and definitions were used:

$$v_r = \langle v_{zg}\rangle^g - \langle v_{zl}\rangle^l, \tag{52}$$

$$K_{VM} = \varepsilon_g \rho_l C_{VM}, \tag{53}$$

$$\varepsilon_l = 1 - \varepsilon_g. \tag{54}$$

5. DYNAMIC ANALYSIS AND VOID WAVE PROPAGATION

Two techniques are commonly used to analyze void wave propagation. These are: (1) evaluation of the eigenvalues (characteristic roots) and eigenvectors of the equation set [11–13], and (2) linearization of the equation set and analysis of the dispersion relation [11,32,34–36]. For real characteristic roots, short wavelength disturbances are stabilized, so the initial-value problem is correctly posed [11]. Complex characteristics may not necessarily indicate an incorrect formulation, but may be attributed to a physical instability of the assumed flow configuration, whereby transition to a different flow pattern may take place [14,15].

5.1. Characteristics for bubbly flows

Equations (48)–(51) constitute the governing set of transient equations for bubbly flow and can be written in the matrix form

$$\boldsymbol{A}\frac{\partial \boldsymbol{U}}{\partial t} + \boldsymbol{B}\frac{\partial \boldsymbol{U}}{\partial z} = \boldsymbol{D}, \tag{55}$$

where $\boldsymbol{U}$ is a column vector of dependent variables given by

$$\boldsymbol{U} = \begin{pmatrix} \varepsilon_g \\ \langle v_{zg}\rangle^g \\ \langle v_{zl}\rangle^l \\ \langle p_l\rangle^l \end{pmatrix}. \tag{56}$$

$\boldsymbol{A}$ and $\boldsymbol{B}$ are matrices given by

$$\boldsymbol{A} = \begin{pmatrix} 1 & 0 & 0 & 0 \\ 1 & 0 & 0 & 0 \\ 0 & (\rho_{\mathrm{g}}\varepsilon_{\mathrm{g}} + K_{\mathrm{VM}}) & -K_{\mathrm{VM}} & 0 \\ 0 & -K_{\mathrm{VM}} & (\rho_{\mathrm{l}}\varepsilon_{\mathrm{l}} + K_{\mathrm{VM}}) & 0 \end{pmatrix}, \tag{57}$$

$$\boldsymbol{B} = \begin{pmatrix} \langle v_{z\mathrm{g}}\rangle^{\mathrm{g}} & \varepsilon_{\mathrm{g}} & 0 & 0 \\ \langle v_{z\mathrm{l}}\rangle^{\mathrm{l}} & 0 & -\varepsilon_{\mathrm{l}} & 0 \\ \langle H_{\mathrm{g}}\rangle_{\mathrm{i}}\sigma & \begin{pmatrix} (\rho_{\mathrm{g}}\varepsilon_{\mathrm{g}} + K_{\mathrm{VM}})\langle v_{z\mathrm{g}}\rangle^{\mathrm{g}} \\ -2\xi\rho_{\mathrm{l}}\varepsilon_{\mathrm{g}}v_r \end{pmatrix} & \begin{pmatrix} 2\xi\rho_{\mathrm{l}}\varepsilon_{\mathrm{g}}v_r \\ -K_{\mathrm{VM}}\langle v_{z\mathrm{l}}\rangle^{\mathrm{l}} \end{pmatrix} & \varepsilon_{\mathrm{g}} \\ -(\xi + k\varepsilon_{\mathrm{g}} - k\varepsilon_{\mathrm{l}})\rho_{\mathrm{l}}v_r^2 & \begin{pmatrix} 2k\rho_{\mathrm{l}}\varepsilon_{\mathrm{g}}\varepsilon_{\mathrm{l}}v_r \\ -K_{\mathrm{VM}}\langle v_{z\mathrm{g}}\rangle^{\mathrm{g}} \end{pmatrix} & \begin{pmatrix} (\rho_{\mathrm{l}}\varepsilon_{\mathrm{l}} + K_{\mathrm{VM}})\langle v_{z\mathrm{l}}\rangle^{\mathrm{l}} \\ -2k\rho_{\mathrm{l}}\varepsilon_{\mathrm{g}}\varepsilon_{\mathrm{l}}v_r \end{pmatrix} & \varepsilon_{\mathrm{l}} \end{pmatrix}, \tag{58}$$

and $\boldsymbol{D}$ is the column vector,

$$\boldsymbol{D} = \begin{pmatrix} 0 \\ 0 \\ -\varepsilon_{\mathrm{g}}\rho_{\mathrm{g}}g - \varepsilon_{\mathrm{g}}F_{\mathrm{D}} \\ -\varepsilon_{\mathrm{l}}\rho_{\mathrm{l}}g + \varepsilon_{\mathrm{g}}F_{\mathrm{D}} \end{pmatrix}. \tag{59}$$

The elements of $\boldsymbol{A}$, $\boldsymbol{B}$ and $\boldsymbol{D}$ are unspecified functions of the components of $\boldsymbol{U}$. The characteristic roots λ of system (55), are obtained by solving the polynomial characteristic equation

$$\det[\boldsymbol{A}\lambda - \boldsymbol{B}] = 0. \tag{60}$$

In general, this equation has four roots. Two of them, which correspond to pressure waves, are not present in our current model, since incompressible fluids only are considered here. The other two roots are determined from the determinant

$$\begin{pmatrix} (\lambda - \langle v_{z\mathrm{g}}\rangle^{\mathrm{g}}) & -\varepsilon_{\mathrm{g}} & 0 & 0 \\ (\lambda - \langle v_{z\mathrm{l}}\rangle^{\mathrm{l}}) & 0 & -\varepsilon_{\mathrm{l}} & 0 \\ -\langle H_{\mathrm{g}}\rangle_{\mathrm{i}}\sigma & \begin{pmatrix} (\lambda - \langle v_{z\mathrm{g}}\rangle^{\mathrm{g}})(\rho_{\mathrm{g}}\varepsilon_{\mathrm{g}} + K_{\mathrm{VM}}) \\ +2\xi\rho_{\mathrm{l}}\varepsilon_{\mathrm{g}}v_r \end{pmatrix} & \begin{pmatrix} -(\lambda - \langle v_{z\mathrm{l}}\rangle^{\mathrm{l}})K_{\mathrm{VM}} \\ -2\xi\rho_{\mathrm{l}}\varepsilon_{\mathrm{g}}v_r \end{pmatrix} & -\varepsilon_{\mathrm{g}} \\ (\xi + k\varepsilon_{\mathrm{g}} - k\varepsilon_{\mathrm{l}})\rho_{\mathrm{l}}v_r^2 & \begin{pmatrix} -(\lambda - \langle v_{z\mathrm{g}}\rangle^{\mathrm{g}})K_{\mathrm{VM}} \\ -2k\rho_{\mathrm{l}}\varepsilon_{\mathrm{g}}\varepsilon_{\mathrm{l}}v_r \end{pmatrix} & \begin{pmatrix} (\lambda - \langle v_{z\mathrm{l}}\rangle^{\mathrm{l}})(\rho_{\mathrm{l}}\varepsilon_{\mathrm{l}} + K_{\mathrm{VM}}) \\ +2k\rho_{\mathrm{l}}\varepsilon_{\mathrm{g}}\varepsilon_{\mathrm{l}}v_r \end{pmatrix} & -\varepsilon_{\mathrm{l}} \end{pmatrix} = 0, \tag{61}$$

which renders a second-order characteristic polynomial with solution:

$$\lambda_{\pm}^{*} = \upsilon \pm \left(\frac{v}{\tau}\right)^{1/2}, \tag{62}$$

where

$$\upsilon = \frac{\varepsilon_{\mathrm{l}}(C_{\mathrm{VM}} - \xi - k\varepsilon_{\mathrm{g}} + \rho_{\mathrm{g}}^{*}\varepsilon_{\mathrm{l}})}{\tau}, \tag{63}$$

$$v = v^2\tau + \varepsilon_g\varepsilon_l(\xi + k - C_{VM}) + \varepsilon_l^2(2\xi - \rho_g^* + H_g^*\sigma^* - C_{VM}), \tag{64}$$

$$\tau = \varepsilon_g\varepsilon_l + C_{VM} + \rho_g^*\varepsilon_l^2, \tag{65}$$

and where the index * has been chosen to indicate the dimensionless forms given by

$$\lambda_\pm^* = \frac{\lambda_\pm - \langle v_{zl}\rangle^l}{\langle v_{zg}\rangle^g - \langle v_{zl}\rangle^l}, \tag{66}$$

$$H_g^*\sigma^* = \frac{\langle H_g\rangle_i\sigma}{\rho_l(\langle v_{zg}\rangle^g - \langle v_{zl}\rangle^l)^2}, \tag{67}$$

$$\rho_g^* = \frac{\rho_g}{\rho_l}. \tag{68}$$

The initial-value hyperbolic equation set is well-posed, provided it possesses real characteristics. The characteristic roots are real, only if $v \geq 0$, if $v < 0$ the characteristic λ^*'s are complex, therefore instabilities should be expected. Algebraic terms do not affect propagation speed. The characteristic velocities are closely related to the fastest and slowest propagation speed of kinematic waves in the system [16].

The evaluation of the interfacial tension effect is based on the potential inviscid flow approximation around bubbles. This is given by [10]

$$M_{gi} = -k_\sigma\rho_l\frac{\partial}{\partial z}[\varepsilon_g(\langle v_{zg}\rangle^g - \langle v_{zl}\rangle^l)^2] - M_{li}, \tag{69}$$

where $k_\sigma = 1/20$. This equation is used similarly as Equation (43). The results are shown in Table II. The results of previous models and a model without interfacial effects are also shown in Table II.

If $k = 0$, $\rho_g^* = 0$ and $H_g^*\sigma^* = 0$, Equations (63)–(65) reduce to the results of Pauchon and Banerjee [13], and if $\rho_g^* = 0$ and $H_g^*\sigma^* = 0$, the model obtained is that of Pauchon and Banerjee [24]. In Lahey's model [32], the interfacial shear stress of the liquid phase is the same order of magnitude as τ_{zzl}^{Re} and interfacial tension effect, which involves the gradient of the void fraction, is not considered. The effect of bubble interaction is considered by Pauchon and Banerjee, [24] through the functionality of C_{VM}, ξ and k with ε_g:

$$C_{VM}(\varepsilon_g) = \frac{2\varepsilon_g + 1}{2\varepsilon_l}; \qquad \xi(\varepsilon_g) = \frac{1 + \varepsilon_g}{4\varepsilon_l}; \qquad k(\varepsilon_g) = \frac{1 + 5\varepsilon_g\varepsilon_l}{5\varepsilon_l^2}. \tag{70}$$

Figure 3 is a map of the characteristic $\lambda_\pm^*$ as a function of void fraction for bubble flows. The domain of hyperbolicity of six models is shown in this graph. The mathematical transition from hyperbolic to non-hyperbolic system ($\lambda_+^* = \lambda_-^*$) is indicative of possible flow transitions (bubble coalescence) according to Ruggles *et al.* [29] Therefore, the model of Pauchon and Banerjee [13] predicts instability or flow transition for $\varepsilon_g > 0.2646$; for Pauchon and Banerjee [24], $\varepsilon_g > 0.4234$ without bubble interaction effects and $\varepsilon_g > 0.1027$ with bubble interaction. Lahey's model [32] predicts instabilities for $\varepsilon_g > 0.3064$. Surface tension effects are found to be very sensitive to instability, which is predicted for $\varepsilon_g > 0.7361$ using Equation (43) with $R_b = 3$ mm and also for $\varepsilon_g > 0.3320$ using Equation (69). The hyperbolicity domain of the present model is reduced when $R_b > 3$ mm. If $R_b \to \infty$ the averaging mean curvature $\langle H_g\rangle_i \to 0$ and the result is reduced to the model of Pauchon and Banerjee [24] without bubble interaction effects. Inclusion of interfacial shear stress also reduces the hyperbolicity domain and is increased with Reynolds stresses. In particular, the hyperbolicity domain is reduced when $C_{VM} > 1/2$ and increased when C_{VM} is smaller. The model without interfacial effects is unstable for $\langle v_{zg}\rangle^g \neq \langle v_{zl}\rangle^l$.

Figure 3 is a map of the characteristic speeds against void fraction for the six models compared in Table II. In reported models by Pauchon and Banerjee [13,24] and by Lahey [32],

Table II. Comparison between models

v	ν	τ	Model
$\varepsilon_l(C_{VM}-\xi-k\varepsilon_g)/\tau$	$v^2\tau+\varepsilon_g\varepsilon_l(\xi+k-C_{VM})+\varepsilon_l^2(2\xi-C_{VM})$ $+\varepsilon_l^2\varepsilon_g\left(\frac{\partial\xi}{\partial\varepsilon_l}+\varepsilon_g\frac{\partial k}{\partial\varepsilon_l}\right)$	$\varepsilon_g\varepsilon_l+C_{VM}$	Pauchon–Benerjee [24] with bubble interaction
$\varepsilon_l(C_{VM}-\xi)/\tau$	$v^2\tau+\varepsilon_g\varepsilon_l(\xi-C_{VM})+\varepsilon_l^2(2\xi-C_{VM})$	$\varepsilon_g\varepsilon_l+C_{VM}$	Pauchon–Banerjee [13]
$\varepsilon_l(C_{VM}-\xi-k\varepsilon_g+\rho_g^*\varepsilon_l)/\tau$	$v^2\tau+\varepsilon_g\varepsilon_l(\xi+k-C_{VM})$ $+\varepsilon_l^2(2\xi-\rho_g^*-C_{VM})-k\varepsilon_g^2\varepsilon_l$	$\varepsilon_g\varepsilon_l+C_{VM}+\rho_g^*\varepsilon_l^2$	Lahey [32]
$\varepsilon_l(C_{VM}-\xi-k\varepsilon_g+\rho_g^*\varepsilon_l+k_g)/\tau$	$v^2\tau+\varepsilon_g\varepsilon_l(\xi+k-C_{VM})$ $+\varepsilon_l^2(2\xi-\rho_g^*-C_{VM}-k_\sigma)$	$\varepsilon_g\varepsilon_l+C_{VM}+\rho_g^*\varepsilon_l^2$	Present work with Equation (69)
$\varepsilon_l(C_{VM}-\xi-k\varepsilon_g)/\tau$	$v^2\tau+\varepsilon_g\varepsilon_l(\xi+k-C_{VM})$ $+\varepsilon_l^2(2\xi-C_{VM})$	$\varepsilon_g\varepsilon_l+C_{VM}$	Pauchon–Benerjee [24] without bubble interaction
$\rho_g^*\varepsilon_l^2/\tau$	$v^2\tau-\rho_g^*\varepsilon_l^2$	$\varepsilon_g\varepsilon_l+\rho_g^*\varepsilon_l^2$	Present work without interfacial effects

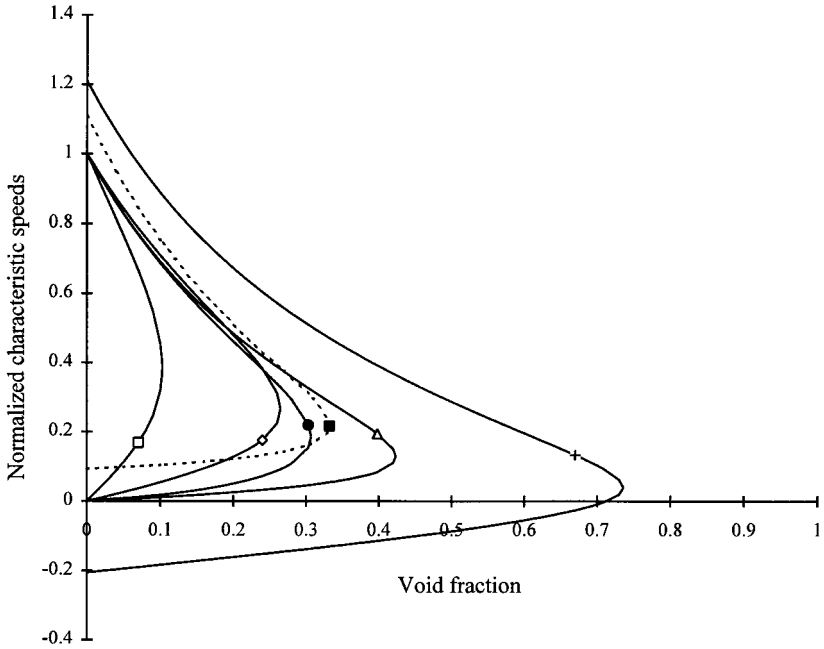

Figure 3. Comparison of void wave models. (□) Pauchon and Banerjee [24] with bubble interaction, (◇) Pauchon and Banerjee [13], (●) Lahey [32], (■) present work with surface tension effect given by Equation (69), (△) Pauchon and Banerjee [24] without bubble interaction, (+) present work with surface tension effect given by Equation (43) and $R_b = 3$ mm.

characteristic speeds between 0 and 1 are found for present simulations, but it should be emphasized that surface tension effects increase characteristic speeds beyond those limits, as observed in Figure 3. Thus, predicted void fraction waves can have characteristic speeds greater than $\langle v_{zg} \rangle^g$ (upper branch of $\lambda_{\pm}^*$, greater than 1) and smaller than $\langle v_{zl} \rangle^l$ (lower branch of $\lambda_{\pm}^*$, less than 0) due to surface tension.

5.2. Void wave propagation

Some experimental data on bubbly air–water flow are available for the model assessment [13,17,18,37,38]. In Figures 4 and 5 respectively, the results of analytical solution with interfacial tension effects (Equation (43)) in explicit form and previous models are compared with experimental data on void propagation from Mercadier [17] and Bernier [18]. In these figures, the y-co-ordinate is kept to the same scale in order to view the differences in the results as the void wave velocity increases.

Bernier's data [18] covers a narrow range of phase average liquid velocity (also known as superficial liquid velocity and represented by j_l), $0 \leq \langle v_{zl} \rangle \leq 0.318$ m s^{-1}, with bubble diameters in the order of 0.5 cm and void fractions ranging from 0 to 0.25. Mercadier's data [17] covers a range of superficial liquid velocity, $-0.05 \leq \langle v_{zl} \rangle \leq 1.0$ m s^{-1} and void fractions ranging from 0 to 0.22.

The two-fluid model is consistent with these data, with the exception of the model with a bubble interaction term, which over estimates void wave propagation. As a consequence, the comparison of void wave analysis with void wave propagation data offers a means to assess dynamic models for interfacial momentum transfer.

Superficial tension effects are found to be very important in determining the hyperbolicity domain and only slightly modify the propagation velocity

6. NUMERICAL SOLUTION PROCEDURE

The governing equations (48)–(51) presented above are a coupled set of partial differential equations (PDE) of the hyperbolic type, for which there are several numerical solution procedures [39–47]. The method of characteristics [39,40,43] is considered to be difficult and tedious to apply, so it has been avoided in favour of the more readily applied finite difference technique which is computationally faster and more flexible than the method of characteristics.

In the present work, transient models and their solution to obtain the velocities, and pressures and void fraction distributions as functions of time and position, are based on finite difference in the implicit scheme. These schemes are used to show the numerical solution

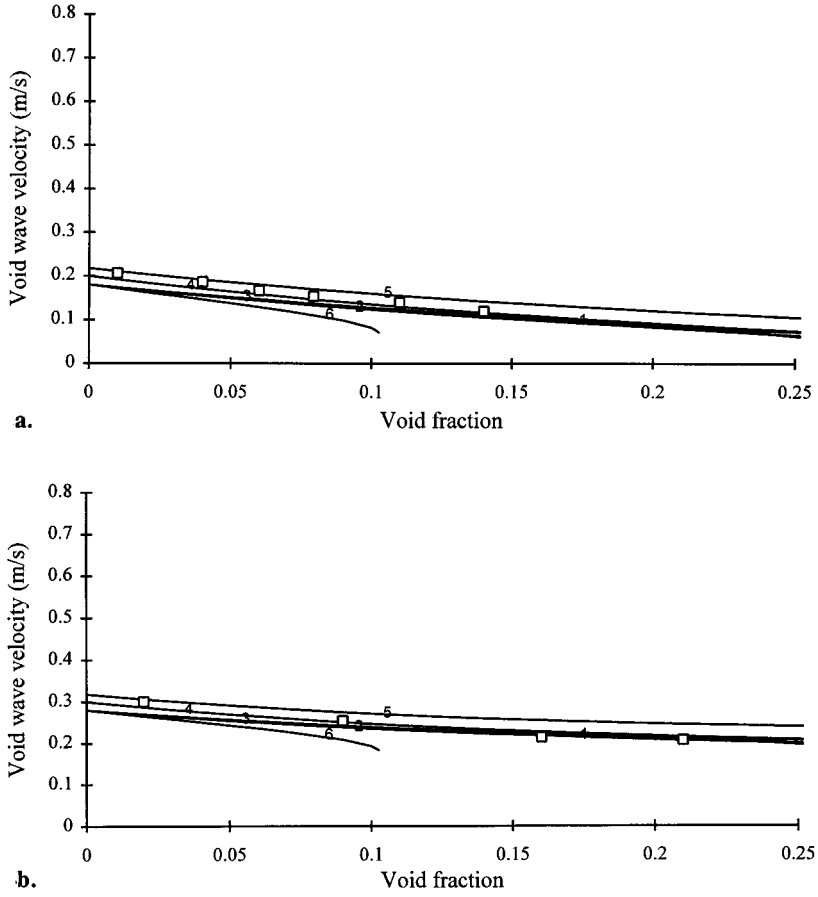

Figure 4. (a) Void wave velocity at $\langle v_{z1} \rangle = 0$ m s^{-1}. (b) Void wave velocity at $\langle v_{z1} \rangle = 0.1$ m s^{-1}. (c) Void wave velocity at $\langle v_{z1} \rangle = 0.2$ m s^{-1}. (d) Void wave velocity at $\langle v_{z1} \rangle = 0.29$ m s^{-1}. (e) Void wave velocity at $\langle v_{z1} \rangle = 0.39$ m s^{-1}. (f) Void wave velocity at $\langle v_{z1} \rangle = 0.49$ m s^{-1}. (□) represents Mercadier's data [17] (1), Lahey [32] (2), Pauchon and Banerjee without bubble interaction [24] (3), Pauchon and Banerjee [13] (4) and (5), with surface tension effects using Equations (69) and (43), respectively, and (6) Pauchon and Banerjee with bubble interaction [24].

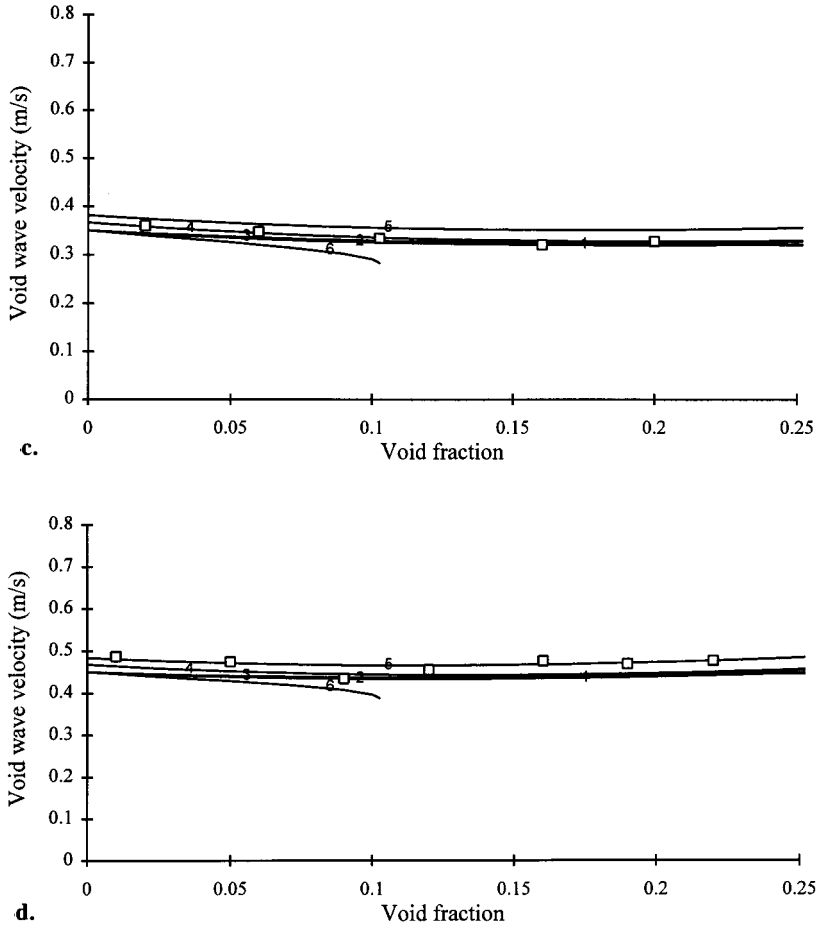

Figure 4 (*Continued*)

procedure, which is easy to programme and validate, using experimental data on void propagation in bubbly flows, taken over several sets of superficial velocity conditions.

In the present solution a one-dimensional mesh centered grid with 100 cells (0.01 m separation between cells) and a variable number of axial elements was used for a column, 1 m in vertical length. The parameters to be determined in each cell are: void fraction, gas velocity, liquid velocity and liquid pressure. The concept of *donor cell* is used for parameter lumping purposes. It states that the fluid exit conditions are same as the fluid conditions in the node itself. Stability of numerical solutions is improved using this concept. The governing equations are solved by a fractional time step in each cell.

6.1. Discretization of the averaged equations

Using the complete set of differential equations developed in previous sections, the discretized forms of these equations are developed. Discretization techniques lead to sparse matrix equations which must be solved at each time step in the simulation. The spatial discretization scheme used is known as a first-order, upstream donor finite difference scheme with a truncation error of order Δz.

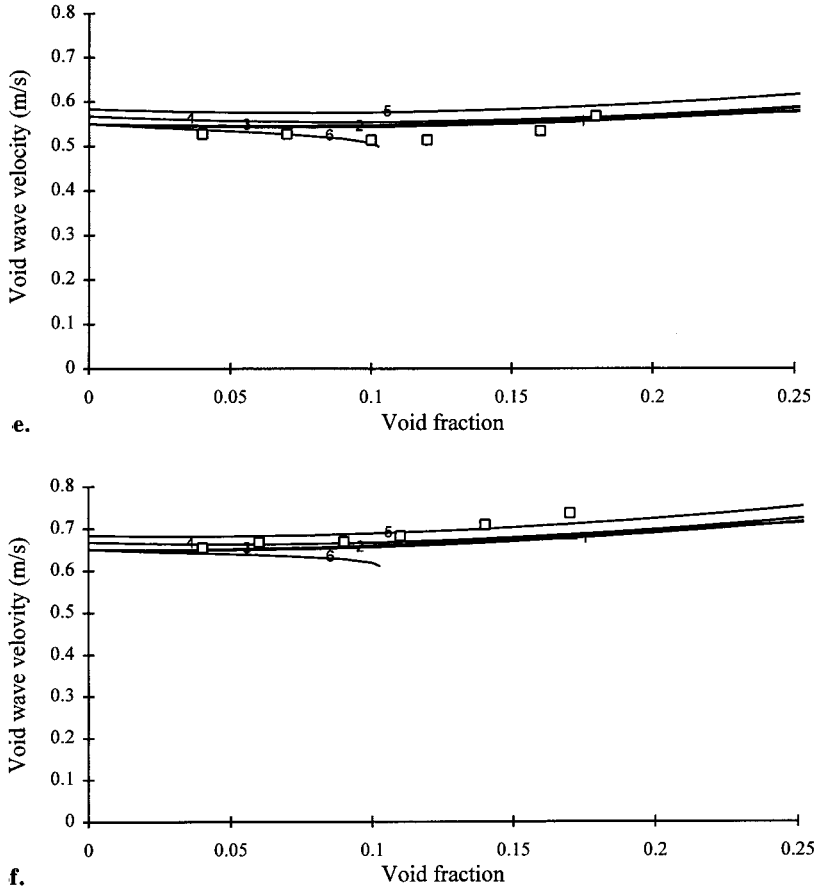

Figure 4 (*Continued*)

The set of equations in discretized form can be written in matrix form as

$$\boldsymbol{A}_j(\boldsymbol{U}_j^o)\boldsymbol{U}_j^{t+\Delta t} = \boldsymbol{B}_j(\boldsymbol{U}_j^o, \boldsymbol{U}_j^t, \boldsymbol{U}_{j-1}^{t+\Delta t}), \tag{71}$$

where Δt is defined as the time step, the indices t and $t+\Delta t$ indicate that the dependent variables are calculated at the old and new times respectively, j is the cell number where the variable is calculated. In this equation, the superscript o represents the dummy variables for the iterative method, $\boldsymbol{U}$ is a column vector of dependent variables given by Equation (56) and matrix $\boldsymbol{A}$ and column vector $\boldsymbol{B}$, are given by

$$\boldsymbol{A}_j = \begin{bmatrix} [\Lambda + (\langle v_{z1}\rangle^1)_j^o] & 0 & -(\varepsilon_1)_j^o & 0 \\ [(\beta_1)_j^o\Lambda + (\beta_2)_j^o] & [-(K_{\mathrm{VM}})_j^o\Lambda + (\beta_5)_j^o] & [(\beta_3)_j^o\Lambda + (\beta_4)_j^o] & (\varepsilon_1)_j^o \\ [\Lambda + (\langle v_{z\mathrm{g}}\rangle^{\mathrm{g}})_j^o] & (\varepsilon_{\mathrm{g}})_j^o & 0 & 0 \\ [(\alpha_1)_j^o\Lambda + (\alpha_2)_j^o] & [(\alpha_3)_j^o\Lambda + (\alpha_4)_j^o] & [(\alpha_5)_j^o - (K_{\mathrm{VM}})_j^o\Lambda] & (\varepsilon_{\mathrm{g}})_j^o \end{bmatrix}, \tag{72}$$

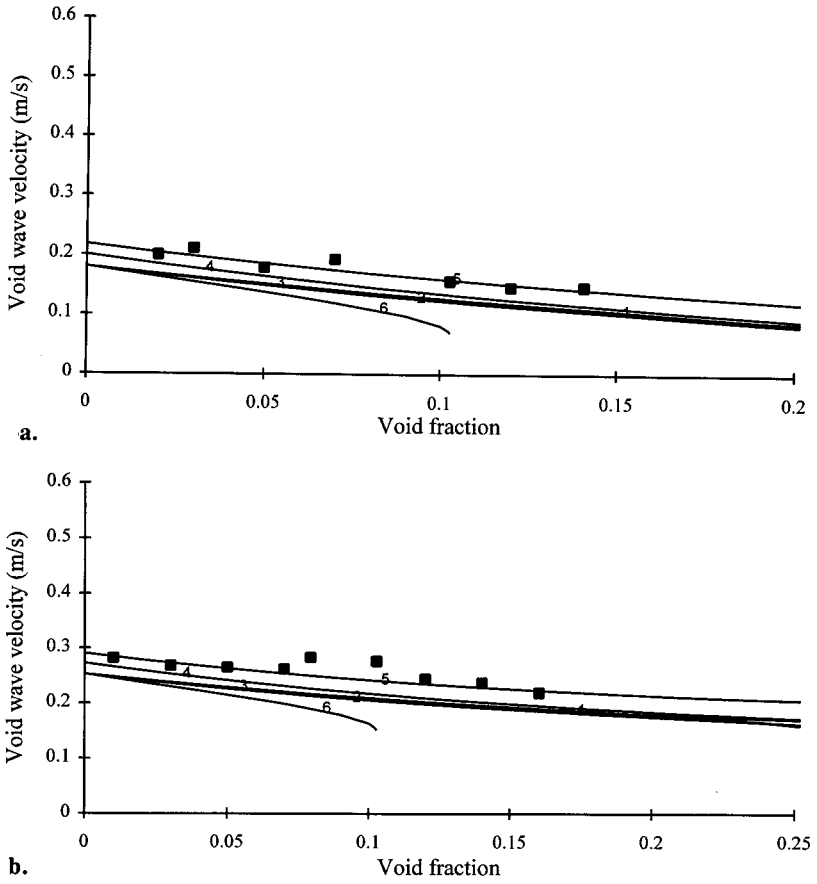

Figure 5. (a) Void wave velocity at $\langle v_{z1}\rangle = 0$ m s^{-1}. (b) Void wave velocity at $\langle v_{z1}\rangle = 0.073$ m s^{-1}. (c) Void wave velocity at $\langle v_{z1}\rangle = 0.169$ m s^{-1}. (d) Void wave velocity at $\langle v_{z1}\rangle = 0.318$ m s^{-1}. (■) denotes Bernier's data [18] (1), Lahey (2), Pauchon and Banerjee without bubble interaction [24] (3), Pauchon and Banerjee [13] (4), and (5) with surface tension effects using Equations (69) and (43) respectively, and (6) Pauchon and Banerjee with bubble interaction [24].

$$\boldsymbol{B}_j = \begin{bmatrix} \Lambda(\varepsilon_g)_j^t + (\langle v_{z1}\rangle^l)_j^o(\varepsilon_g)_{j-1}^{t+\Delta t} - (\varepsilon_l)_j^o(\langle v_{z1}\rangle^l)_{j-1}^{t+\Delta t} \\ (\beta_1)_j^o\Lambda(\varepsilon_g)_j^t + (\beta_2)_j^o(\varepsilon_g)_{j-1}^{t+\Delta t} - (K_{VM})_j^o\Lambda(\langle v_{zg}\rangle^g)_{j-1}^t + (\beta_5)_j^o(\langle v_{zg}\rangle^g)_{j-1}^{t+\Delta t} \\ + (\varepsilon_l)_j^o(\langle p_l\rangle^l)_{j-1}^{t+\Delta t} + (\beta_3)_j^o\Lambda(\langle v_{z1}\rangle^l)_j^t + (\beta_4)_j^o(\langle v_{z1}\rangle^l)_{j-1}^{t+\Delta t} + (\varepsilon_g)_j^o[(F_D)_j^o - \rho_l g]\Delta z \\ \Lambda(\varepsilon_g)_j^t + (\langle v_{zg}\rangle^g)_j^o(\varepsilon_g)_{j-1}^{t+\Delta t} + (\varepsilon_g)_j^o(\langle v_{zg}\rangle^g)_{j-1}^{t+\Delta t} \\ (\alpha_1)_j^o\Lambda(\varepsilon_g)_j^t + (\alpha_2)_j^o(\varepsilon_g)_{j-1}^{t+\Delta t} + (\alpha_3)_j^o\Lambda(\langle v_{zg}\rangle^g)_j^t + (\alpha_4)_j^o(\langle v_{zg}\rangle^g)_{j-1}^{t+\Delta t} \\ - (K_{VM})_j^o\Lambda(\langle v_{z1}\rangle^l)_j^t + (\alpha_5)_j^o(\langle v_{z1}\rangle^l)_{j-1}^{t+\Delta t} + (\varepsilon_g)_j^o(\langle p_l\rangle^l)_{j-1}^{t+\Delta t} - (\varepsilon_g)_j^o[(F_D)_j^o + \rho_g g]\Delta z \end{bmatrix} \quad (73)$$

where $\Lambda = \Delta z/\Delta t$.

The implicit scheme, results in a set of non-linear equations, which can be solved with some iterative method. In Equation (71), the variables with indices $j-1$ and t are known, since these are the inlet variables and the initial condition, respectively.

The numerical solution of Equation (71) is obtained using the LINPACK program [48], which is a numerical code for solving simultaneous linear equations. The algorithm on which this program is based, is the factorization of a matrix using a version of Gaussian elimination

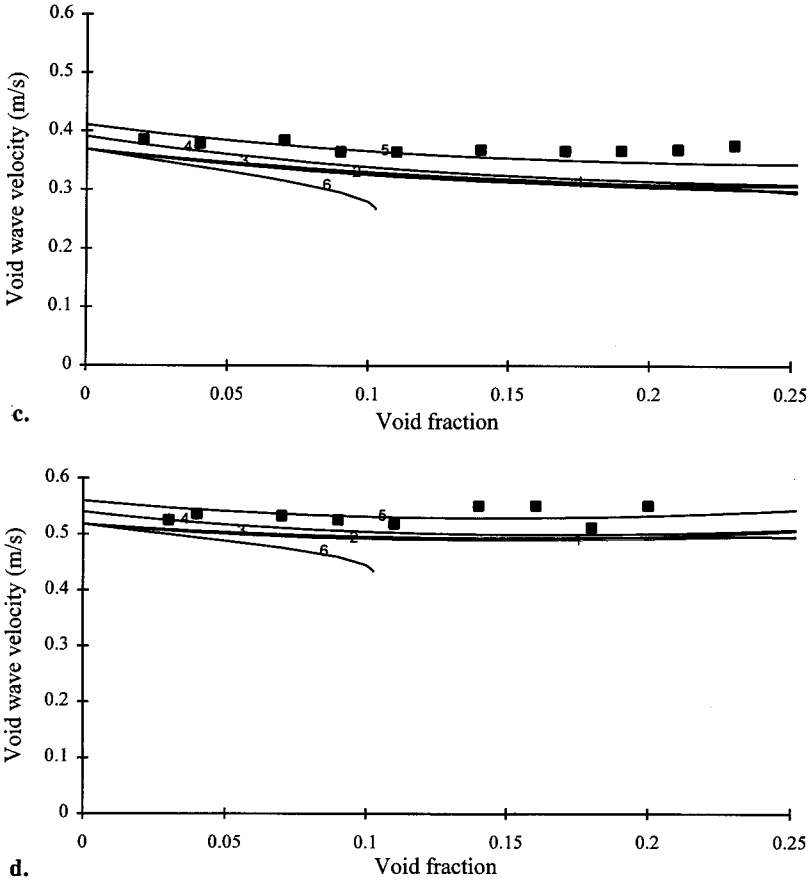

Figure 5 (*Continued*)

with partial pivoting. It is necessary, however, to specify the initial conditions, boundary conditions and properties of fluid phases. This was done for the following values.

6.1.1. Initial condition. At time $t = 0$, particularizing the initial condition for all cells is specified, for the following variables: $(\varepsilon_g)_j^t$, $(\langle v_{zg} \rangle^g)_j^t$, $(\langle v_{zl} \rangle^l)_j^t$.

6.1.2. Boundary conditions. There are entrance values to the system, and these are either constant or functions of time. These values are: $(\varepsilon_g)_e$, $(\langle v_{zg} \rangle^g)_e$, $(\langle v_{zl} \rangle^l)_e$, $(\langle p_l \rangle^l)_e$, where the index e is used to indicate entrance to the system.

6.1.3. Physical parameters. Air density ρ_g, water density ρ_l and surface tension σ.

6.2. Solution procedure

Step 1. Assign entrance values to the first cell ($j = 1$): $\boldsymbol{U}_1 = \boldsymbol{U}_e$.
Step 2. Assign the initial condition at $t = 0$ to variables with index o, for all cells: $\boldsymbol{U}_j^o = \boldsymbol{U}_j^t$.
Step 3. Each element of the matrix $\boldsymbol{A}$ (Equation (72)) and each element of the column vector $\boldsymbol{B}$ (Equation (73)) are calculated using the initial condition given in Step 2.
Step 4. Using the numerical code LINPACK [48], the vector solution $\boldsymbol{U}_j^{t+\Delta t}$ is obtained.

Step 5. The iterative process for solving problems in two-phase flow is performed using discretized forms of the mass and momentum equations for each phase. If the condition $[\boldsymbol{A}_j \boldsymbol{U}_j^{t+\Delta t} - \boldsymbol{B}_j] \leq |\text{error}|$ is not satisfied, the process is restarted from Step 2, but this time assigning $\psi_j^o = (\psi_j^t + \psi_j^{t+\Delta t})/2$, until convergence is obtained. The method requires four iterations at most (low flow) for convergence with $\Delta z = 0.01$ m and $\Delta t = 0.01$ s.

Step 6. The process described in Steps 2–5 is repeated from cell $j = 3$ to cell $j = n$. The variables calculated in cell $j = 2$ are the entrance variables of cell $j = 3$ and so on successively, until the entrance variables for cell $j = n$ are calculated at of the cell $j = n - 1$.

Step 7. When all cells are computed, the variables calculated at the new time $t + \Delta t$, are assigned to the variables at time t: $\boldsymbol{U}_j^t = \boldsymbol{U}_j^{t+\Delta t}$, and the process is restarted from Step 2 until the total simulation time is reached.

The implantation of this numerical solution procedure in a computer program is straightforward. However, it should be stressed that matrix $\boldsymbol{A}$ is close to being computationally singular and the solution could be inaccurate. With appropriate matrix scaling, this problem was solved.

7. NUMERICAL RESULTS AND DISCUSSION

Interfacial terms are an essential feature of momentum balances. If the only interfacial terms considered are the interfacial pressure difference for the liquid phase and the interfacial drag force, a numerical basic solution can be obtained. This solution presents a decaying pattern for liquid velocity and void fraction, as well as an increasing pattern for gas velocity. The combination of both patterns is an indication of a pronounced slippage between the phases. Other interfacial and bulk mechanisms can be additionally considered. Thus, Reynolds stresses only slightly modify the basic solution. Conversely, added mass terms contribute highly to reduce slip between phases, since added mass term involves both the deceleration of the gas phase by the liquid and the continuation of liquid by gas bubbles. In addition, viscous effects (bulk effects) do not appreciably change the numerical results, while added mass effects greatly improve numerical stability.

7.1. Void wave velocity

The transient and steady state phenomena in two-phase flow are controled by the propagation of void waves (e.g. choking, flooding, void shocks, density wave instabilities, and flow regime transition). Void waves strongly depend on the closure relationships used in two-fluid models [13,24,29,32,35]. In the previous section the eigenvalues of the equation set are evaluated in order to analyze void wave propagation, but in the present section the propagation of void waves is obtained with a numerical approach.

Void wave propagation speed can be computed from numerical simulation by defining a travel time of the void wave from a level N of the column to another level $N + 1$. The following cross-correlation function was defined for that purpose:

$$R_{xy}(N, \tau_j) = \sum_{i=1}^{m-j} [\varepsilon_g(N+1, t_{i+j}) - \varepsilon_g(N, t_i)]^2, \tag{74}$$

where t_i; $i = 1, \ldots m$, is a succession of time instants where the values of void fraction were recorded. τ_j; $j = 1, \ldots n$ $(n < m)$ is a succession of time delays. The travel time is defined as the value of τ_j when $R_{xy}(N, \tau_j)$ reaches its minimum value. Then the void wave speed is defined as the ratio of the distance between levels N and $N + 1$ to the travel time previously found.

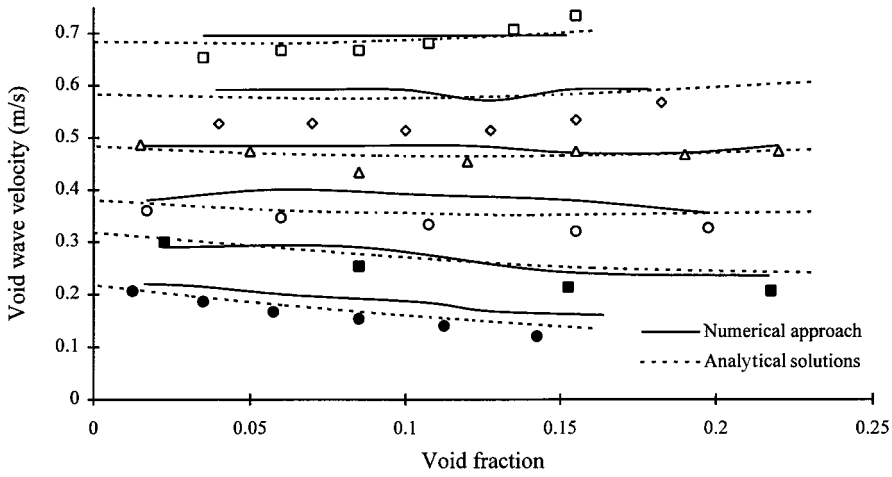

Figure 6. Void wave velocity as a function for ε_g for different values of the liquid superficial velocity from Mercadier [17]. (●) $\langle v_{zl} \rangle = 0.0.0$ m s^{-1}, (■) $\langle v_{zl} \rangle = 0.1$ m s^{-1}, (○) $\langle v_{zl} \rangle = 0.2$ m s^{-1}, (△) $\langle v_{zl} \rangle = 0.29$ m s^{-1}, (◇) $\langle v_{zl} \rangle = 0.39$ m s^{-1}, (□) $\langle v_{zl} \rangle = 0.49$ m s^{-1}.

The dynamic tests were performed for $\varepsilon_g \geq 0$. In these tests, the superficial liquid velocity $\langle v_{zl} \rangle$ (phase average liquid velocity) was kept constant while the superficial gas velocity $\langle v_{zg} \rangle$ was perturbed around a steady state. The transient behavior of ε_g was numerically calculated in the levels N and $N+1$ for a set of times t_i; $i = 1, \ldots m$, in order to obtain the wave propagation speed using the cross-correlation function given by Equation (74).

In Figures 6 and 7 the results from the numerical approach of the model for the interphase forces in bubbly flow are shown, and are compared with experimental data [17,18] and analytical solutions on void propagation. The two-phase model with interfacial tension is in agreement with these data and analytical solutions.

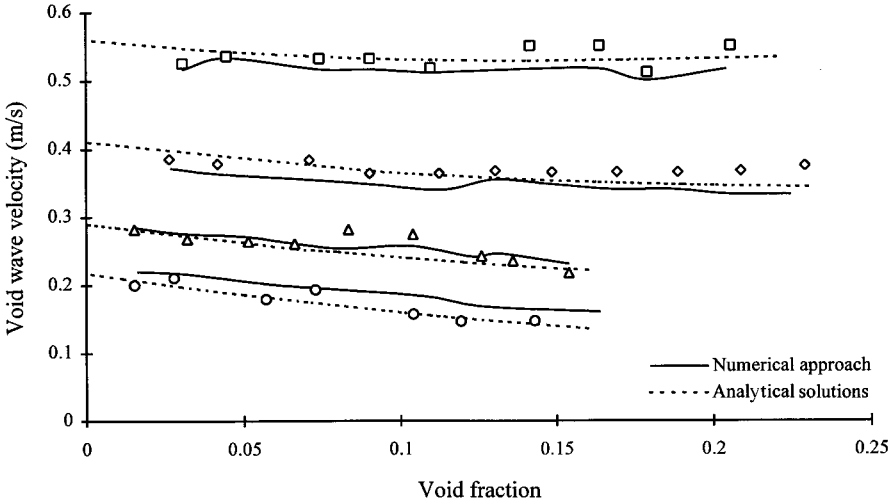

Figure 7. Void wave velocity as a function of ε_g for different values of the liquid superficial velocity from Bernier [18]. (○) $\langle v_{zl} \rangle = 0.0$ m s^{-1}, (△) $\langle v_{zl} \rangle = 0.073$ m s^{-1}, (◇) $\langle v_{zl} \rangle = 0.169$ m s^{-1}, (□) $\langle v_{zl} \rangle = 0.318$ m s^{-1}.

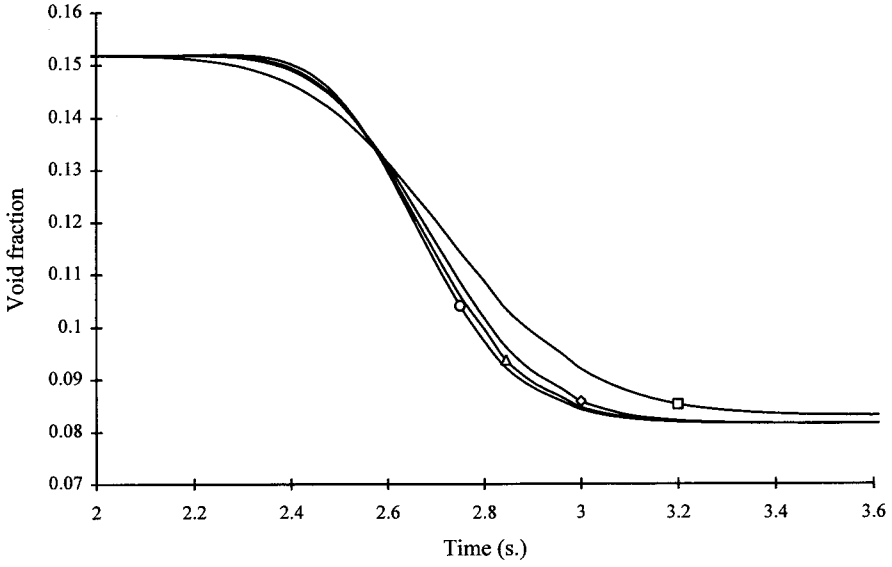

Figure 8. Momentum interfacial and bulk effects in transient conditions. (◇) Complete effects, (□) without surface tension effects, (△) without Reynolds stress effects, (○) without interfacial averaged pressure effects.

7.2. Interfacial and bulk effects

The importance of interfacial and bulk effects in transient condition is studied. The transient state is produced from a basic steady state condition with values $\varepsilon_g = 0.1518$, $\langle v_{zg} \rangle = 0.0488$ m s^{-1} and $\langle v_{zl} \rangle = 0.1$ m s^{-1}. At 1 s, the superficial gas velocity is disturbed to $\langle v_{zg} \rangle = 0.0275$ m s^{-1} and the following contributions to the model are analyzed:

- full model, with complete interfacial and bulk effects,
- without surface tension effects,
- without Reynolds stress effects,
- without interfacial averaged pressure effects,

In Figure 8, the behaviors of void fraction for the several cases are shown. If Reynolds stress effects are not considered for a time greater than 2.6 s, the void fraction changes are locally accelerated. Thus, Reynolds stress effects slightly modify the basic solution. If interfacial averaged pressure effects are not considered for time greater than 2.6 s, the void fraction changes are also locally accelerated and the contribution of this effect is greater than Reynolds stress effects, as it can be seen in Figure 8. Conversely, if surface tension effects are not considered, the void fraction changes are locally delayed. This effect contributes highly to modify the kinematic wave structure. Without considering surface tension, the void wave speed was 0.262 m s^{-1} and the void fraction reached in the new steady state was 0.0831, but in the other three cases, the void wave velocity was 0.271 m s^{-1} and the void fraction for final state was 0.0816. Moreover, it was found that interfacial pressure effects and surface tension effects are greatly significant. This fact may be a valuable indication for further modeling, since surface tension effects have not been considered by previous analyses on void propagation in bubbly flows. It should be stressed that for times smaller than 2.6 s, the opposite behavior of analyzed effects could be observed.

The same test was performed for a constant $\langle v_{z1} \rangle = 0.49$ m s^{-1}. The behavior of the void fraction was found to be practically invariant for changes in $\langle v_{zg} \rangle$. This behavior can be understood, because the dynamic motion of mixture is controled by convective effects. Therefore, interfacial and bulk effects are only important for low superficial liquid velocity.

8. CONCLUSIONS

A set of general volume averaged mass and momentum transport equations with surface tension and interfacial pressure effects to describe bubble flow behavior in both steady and transient conditions was developed. Moreover, a very simple, faster and more stable numerical solution procedure with respect to previous works, was modified in order to numerically solve the one-dimensional two-fluid model, using the upstream donor cell finite difference technique in the implicit scheme. A dynamic analysis rendered a map for the characteristic values and showed that influence of interfacial tension effects is a very important contribution in the definition of the domain of hyperbolicity (stable region), and predicted void fraction waves with characteristic speeds greater than intrinsic average gas velocity and smaller than intrinsic average liquid velocity. A comparison of the results of this study with experimental data and characteristic velocities (analytical solutions) suggested that the numerical approach developed is an appropriate technique for the analysis of void wave propagation, and offers a means for model assessment. The numerical results in transient tests demonstrate that the surface tension effect causes the acceleration of void fraction waves. Consideration of interfacial pressure and Reynolds stress effects cause the deceleration of these void fraction waves. The surface tension effect is more important at low superficial liquid velocities (≈ 0.1 m s^{-1}) than at higher ones (≈ 0.49 m s^{-1}).

ACKNOWLEDGMENTS

The authors would like to thank CONACyT, México, for financial support through the Research Grant No. 400200-5-3444A.

REFERENCES

1. J.C. Slattery, 'Flow of viscoelastic fluids through porous media', *AIChE J.*, **13**, 1066–1071 (1967).
2. S. Whitaker, 'Diffusion and dispersion in porous media', *AIChE J.*, **13**, 420–427 (1967).
3. W.G. Gray and P.C.Y. Lee, 'On the theorems for local volume averaging of multiphase systems', *Int. J. Multiphase Flow*, **3**, 333–340 (1977).
4. F.A. Howes and S. Whitaker, 'The spatial averaging theorem revisited', *Chem. Eng. Sci.*, **40**, 1387–1392 (1985).
5. A. Soria and H.I. de Lasa, 'Averaged transport equations for multiphase systems with interfacial effects', *Chem. Eng. Sci.*, **46**, 2093–2111 (1991).
6. S. Whitaker, 'Advances in the theory of fluid motion in porous media', *Ind. Eng. Chem.*, **61**, 14–28 (1969)
7. A. Biesheuvel and L. Wijngaarden, 'Two-phase flow equations for a dilute dispersion of gas bubbles in liquid', *J. Fluid Mech.*, **148**, 301–318 (1984).
8. S. Whitaker, 'The closure problem for two-phase flow in homogeneous porous media', *Chem. Eng. Sci.*, **49**, 765–780 (1994).
9. S. Whitaker, 'Flow in porous media I: A theoretical derivation of Darcy's law', *Transp. Porous Media*, **1**, 3–25 (1986).
10. D.A. Drew, 'Analytical modeling of multiphase flows', in R.T. Lahey Jr. (ed.), *Boiling Heat Transfer: Modern Developments and Advances*, Elsevier, New York, 1992, pp. 56–68.
11. J.D. Ramshaw and J.A. Trapp, 'Characteristic, stability, and short-wavelength phenomena in two-phase flow equation system', *Nucl. Sci. Eng.*, **66**, 93–102 (1978).
12. A. Biesheuvel and L. Van Wijngaarden, 'Two-phase flow equations for a dilute dispersion of gas bubbles in liquid', *Appl. Sci. Res.*, **38**, 297–303 (1984).

13. C. Pauchon and S. Banerjee, 'Interphase momentum interaction effects in the averaged multifield model, Part I: Void propagation in bubbly flows', *Int. J. Multiphase Flow*, **12**, 559–573 (1986).
14. A. Soria and H.I. de Lasa, 'Averaged topological equations for dispersed two-phase flow', *Int. J. Multiphase Flow*, **18**, 943–964 (1992).
15. N. Brauner and M.D. Maron, 'Stability analysis of stratified liquid–liquid flow', *Int. J. Multiphase Flow*, **18**, 103–121 (1992).
16. G.B. Whitham, *Linear and Nonlinear Waves*, Wiley, New York, 1974
17. Y. Mercadier, 'Contribution a l'etudes des propagations de perturbation de taux de vice dans les ecoulements diphasiques eau–air a bulles', *Docteur Engenieur*, *Thesis*, L'Universite Scientifique et Medicale & L'Institut National Polytechnique de Grenoble, 1981.
18. R.J.N. Bernier, 'Unsteady two-phase flow instrumentation and measurement', *Ph.D. Thesis*, California Institute of Technology, 1982.
19. R.T. Lahey, L.Y. Cheng, D.A. Drew and J.E. Flaherty, 'The effect of virtual mass on the numerical stability of accelerating two-phase flow', *Int. J. Multiphase Flow*, **6**, 281–294 (1980).
20. J.M. Delhaye, 'Basic equations for two phase flow modeling', in A.E. Bergles, J.G. Collier, J.M. Delhaye, G.F. Hewitt and F. Mayinger, (eds.), *Two-Phase Flow and Heat Transfer in the Power and Process Industries*, Hemisphere, Washington, DC, 1981, pp. 40–97.
21. M. Hassanizadeh and W.G. Gray, 'General conservation equations for multiphase systems: 1 Averaging procedure', *Adv. Water Resour.*, **2**, 131–144 (1979).
22. W.G. Gray, 'A derivation of the equations for multiphase transport', *Chem. Eng. Sci.*, **30**, 229–233 (1975).
23. D.A. Drew and R.T. Lahey Jr., 'Application of general constitutive principles to the derivation of multidimensional two phase equations', *Int. J. Multiphase Flow*, **5**, 243–264 (1979).
24. C. Pauchon and S. Banerjee, 'Interphase momentum interaction effects in the averaged multifield model, Part II: Kinematic waves and interfacial drag in bubbly flows', *Int. J. Multiphase Flow*, **12**, 559–573 (1988).
25. S. Banerjee and M.C. Chan, 'Separated flow models I: Analysis of the averaged and local instantaneous formulations', *Int. J. Multiphase Flow*, **6**, 1–24 (1980).
26. R.T. Lahey Jr. and D.A. Drew, 'The three-dimensional time and volume averaged conservation equations of two-phase flow', *Adv. Nucl. Sci. Technol.*, **20**, 1–69 (1989).
27. M. Ishii and M. Mishima, 'Two-fluid model and hydrodynamic constitutive relations', *Nucl. Eng. Des.*, **82**, 107–126 (1984).
28. T.Z. Harmathy, 'Velocity of large drops and bubbles in media of infinite or restricted extent', *AIChE. J.*, **2**, 281–288 (1960)
29. A.E. Ruggles, R.T. Lahey Jr. and D.A. Drew, 'An analysis of void wave propagation in bubbly flows', *Proc. 15th Miami Intl. Symp.*, *Multiphase Transport and Particulate Fenomena*, 1988, pp. 175–192.
30. D.A. Drew and R.T. Lahey Jr., 'The virtual mass and lift force on a sphere in rotating and straining inviscid flow', *Int. J. Multiphase Flow*, **13**, 333–340 (1987).
31. C. Pauchon and P. Smereka, 'Momentum interactions in dispersed flow: An averaging and variational approach', *Int. J. Multiphase Flow*, **18**, 65–87 (1992).
32. R.T. Lahey, 'Void wave propagation phenomena in two-phase flow (Kern award lecture)', *AIChE J.*, **37**, 123–135 (1991).
33. M. Ishii, *Thermo-Fluid Dynamic Theory of Two Phase Flow*, Eyrolles, Paris, 1975.
34. A. Biesheuvel and C. M. Gorissen, 'Void fraction disturbances in a uniform bubbly fluid', *Int. J. Multiphase Flow*, **16**, 211–231 (1990).
35. J.-W. Park, D.A. Drew, R.T. Lahey Jr. and A. Clausse, 'Void wave dispersion in bubbly flows', *Nucl. Eng. Des.*, **121**, 1–10 (1990).
36. P.E. Lisseter and A.C. Fowler, 'Bubbly flow-II, modelling void fraction waves', *Int. J. Multiphase Flow*, **18**, 205–215 (1992).
37. J.M. Saiz-Jabardo and J.A. Bouré, 'Experiments on void fraction waves', *Int. J. Multiphase Flow*, **15**, 483–493 (1989).
38. A. Soria, and H.I. de Lasa, 'Kinematics waves and flow patterns in bubble columns and three-phase fluidized beds', *Chem. Eng. Sci.*, **47**, 3403–3110 (1992).
39. J.M. González-Santaló and R.T. Lahey Jr., 'An exact solution for flow transients in two-phase systems by the method of characteristics', *ASME*, *Paper 75-WA/HT-25*, 470–476 (1973).
40. R.W. Lyczkowski, D. Gidaspow, C.W. Solbrig and E.D. Hughes, 'Characteristic and stability analyses of transient one-dimensional two-phase flow equations and their finite difference approximations', *ASME*, *Paper 75-WA/HT-23*, 1–15 (1975).
41. J.R. Travis, F.H. Harlow and A. Amdsen, 'Numerical calculation of two-phase flows', *Nucl. Sci. Eng.*, **61**, 1–10 (1976).
42. R. Martini, G.C. Pierini and C. Sandri, 'A one-dimensional transient two-phase flow model and its implicit finite-difference solution', in *Proc. CSNI Specialists Meeting on Transient Two-Phase Flow*, Toronto, 1978, pp. 379–397.
43. R.L. Ferch, 'Method of characteristics solutions for non-equilibrium transient flow-boiling', *Int. J. Multiphase Flow*, **5**, 265–279 (1979).

44. W.T. Hancox, R.L. Ferch, W.S. Liu and R.E. Nieman, 'One-dimensional models for transient gas–liquid flows in ducts', *Int. J. Multiphase Flow*, **6**, 25–40 (1980).
45. J.G.M. Andersen and J.C. Shaug, 'A predictor method for the BWR version of the TRAC computer code', in N.M. Farukhi (ed.), *AIChE Symposium Series*, **80**, 275–280 (1984).
46. J.M. Doster, 'Numerical solutions of multiphase flow problems', in A. Sharon and M.R Facory, (eds.), *Simulators VI*, **21**, 59–66 (1989).
47. K. Minami and O. Shoham, 'Transient two-phase flow behavior in pipelines—experiment and modeling', *Int. J. Multiphase Flow*, **4**, 739–752 (1994).
48. J.J Dongarra, J.R. Bunch, C.B. Moler and G.W. Stewart, 'LINPACK user guide', *Soc. Ind. Appl. Math.*, 1990.
49. S.K. Wang, S.J. Lee, O.C. Jones and R.T. Lahey, '3-D turbulence structure and phase distribution measurements in bubbly two-phase flows', *Int. J. Multiphase Flow*, **13**, 327–343 (1987).

